

## EFFECT OF ETHANOL FUEL AND MICROBIOLOGICALLY INFLUENCED CORROSION ON THE FATIGUE CRACK GROWTH BEHAVIOR OF PIPELINE STEELS\*

\*Contribution of NIST, an agency of the US government. Not subject to copyright.

Jeffrey W. Sowards  
T. Dash Weeks  
J. David McColskey  
James R. Fekete  
NIST, Materials Reliability Division  
325 Broadway  
Boulder, CO 80305  
U.S.A.

Luke Jain  
Colorado School of Mines  
Dept. of Metallurgical & Materials Engineering  
Golden, CO 80401  
U.S.A.

Chase Williamson  
Colorado School of Mines  
Dept. of Environmental Science & Engineering  
Golden, CO 80401  
U.S.A.

### ABSTRACT

Ethanol fuel production and consumption are expected to increase significantly in the near future. Existing pipeline infrastructure could be repurposed to transport ethanol and other biofuels from production sources, such as those located in the Midwest, to end users across the country. The effects of ethanol fuel, including its ability to harbor corrosion-inducing microbiological life, are not well established in relation to degrading the fatigue properties of pipeline materials. In this work experiments were performed to evaluate crack growth behavior of pipeline steels in several ethanol environments. The environments included a simulated fuel grade ethanol and an ethanol-water solution inoculated with a microbiological species (*Acetobacter acetii*) isolated from industrial ethanol storage tanks. Fatigue crack growth rates of API 5L X52 and X70 pipeline steels were determined as a function of the stress intensity amplitude ( $\Delta K$ ) during exposure to the various ethanol environments. Significant increases in fatigue crack growth rate were found above  $\Delta K$  levels of approximately 17 MPa·m<sup>1/2</sup> and 20 MPa·m<sup>1/2</sup> during testing of X52 and X70 in simulated fuel grade ethanol, respectively. Fatigue crack growth rates were increased by almost two orders of magnitude, relative to air, during testing of X52 and X70 in ethanol-water solutions inoculated with acetic acid producing bacteria. Concurrent research suggested that glutaraldehyde may be an effective biocide for controlling acid producing bacteria in pipelines. The data presented are useful for reliability models to ensure safe fuel transport of ethanol.

Key words: Acid producing bacteria; biofuel; fatigue crack growth; fuel grade ethanol; microbiologically influenced corrosion; pipeline steel; X52; X70.

## INTRODUCTION

The rates of production and consumption of ethanol, biodiesel, and other alternative fuels are projected to increase significantly in the near future<sup>[1]</sup>. However, much of the current biofuel is produced in the midwestern U.S. and transported by railcar to end-user destinations. This transportation system may become cost-prohibitive for future expansion of ethanol as a widely used energy source. Existing pipelines could be repurposed to promote more widespread use of biofuels and lower their transportation costs. However, pipeline transport of ethanol and other biofuels poses potential problems due to corrosion-related damage.

Several investigations have shown that pipeline steels are susceptible to a particular type of environmentally assisted fracture during ethanol exposure known as ethanol stress corrosion cracking (SCC)<sup>[2-5]</sup>. Studies have shown that high chloride and oxygen content and low pH exacerbate ethanol SCC susceptibility. Acetic acid production by alcohol oxidation at stress corrosion crack tips has been suggested as a possible mechanism to promote SCC<sup>[6]</sup>. Additions of acetic acid to ethanol fuel have been shown to increase SCC susceptibility of pipeline steels<sup>[3,7]</sup>. Several other qualitative models have been proposed to explain ethanol SCC. The models suggest that anodic dissolution is enhanced at growing crack tips that are deaerated by fresh metal exposed during plastic flow<sup>[5,8]</sup>. These SCC models may have applicability in explaining fatigue crack growth behavior of pipeline steels during exposure to ethanol fuel environments.

Microbial contamination and corrosion has long been associated with distribution and use of a variety of liquid fuels<sup>[9]</sup>. Ethanol fuels sampled from industrial user storage tanks have been reported to harbor microbiological life, including phyla that contain both acid producing bacteria (APB) and sulfate reducing bacteria (SRB)<sup>[10]</sup>. Species from both bacteria classifications have been shown to promote microbiologically influenced corrosion (MIC)<sup>[11]</sup>. Pope *et al.* showed that APB promoted localized corrosion of natural-gas pipeline steel at inclusion sites<sup>[12]</sup>. The observed corrosion damage was distinct from corrosion produced by protic acid (including that produced by SRB and H<sub>2</sub>SO<sub>4</sub>) of the same pH. A mechanism was suggested whereby acetate ions formed complexes with iron, which lead to a significant role in the corrosion process<sup>[12]</sup>. Other studies<sup>[13-14]</sup> have reported a significant increase in fatigue crack growth rates (FCGR) of high-strength steels (RQT 501<sup>[13]</sup>, RQT 701<sup>[13]</sup>, and HY 130<sup>[14]</sup>) exposed to seawater environments containing microbiological agents such as SRB. In addition to a microbiological effect, FCGRs of a high strength steel (667 MPa yield strength) were reported to increase significantly in ethanol solutions containing increasing concentrations of water<sup>[15]</sup>. However, there are limited FCGR data available that demonstrate the effect of biofuel exposure and associated microbiological species on steels relevant to pipeline transport.

The experiments in this work evaluated the effect of ethanol fuel environments, including those with microbiologically active species, on the FCGR behavior of pipeline steels. Data generated in this work are critical for sound engineering prediction of fatigue crack growth behavior during transport of ethanol fuels in steel pipelines.

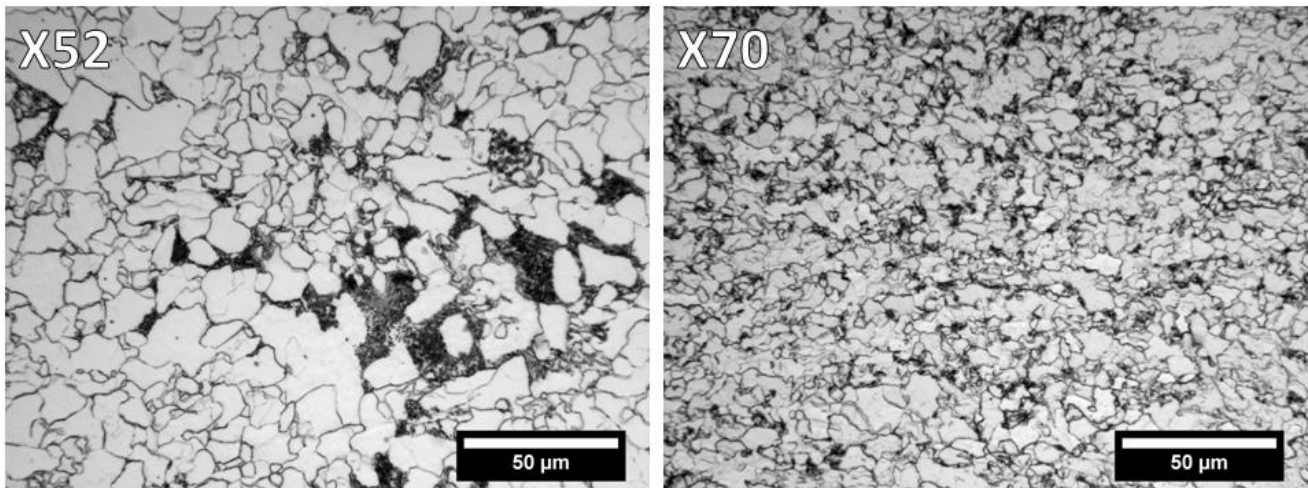
## MATERIALS AND METHODS

Two grades of pipeline steel (API 5L X52 and X70) were obtained for this study. Chemical compositions of both alloys are shown in Table 1. Metallographic specimens from the pipeline materials were prepared with standard methods for optical microscopy (1 μm final polish and 2% nital etch). Representative microstructures of both materials are shown in Figure 1. The API 5L X52 contains a mixture of polygonal ferrite and pearlite and X70 contains a fine-grained polygonal ferrite and bainitic structure.

**Table 1: Chemical Composition of API 5L X52 and X70 Steels (Wt. %)**

Alloy	Fe	C	Si	Cr	Ni	Mn	Cu	Mo	Nb	Ti	Al	V	S	P
X52	Bal.	0.070	0.195	0.030	0.020	1.050	0.050	0.004	0.021	0.001	0.029	0.003	0.008	0.008
X70	Bal.	0.050	0.185	0.043	0.017	1.505	0.030	0.010	0.084	0.015	0.032	0.010	0.006	0.012

Tensile and compact tension (C(T)) specimens were machined from pipe sections in the longitudinal orientation from both grades. Tensile tests were performed according to ASTM E8<sup>[16]</sup> standard test methods with a 250 kN (55 kip) load capacity servohydraulic test frame. FCGR measurements were performed with the compliance technique according to ASTM E647<sup>[17]</sup> with two 100 kN (22 kip) load capacity servohydraulic test frames. Crack growth rates (da/dN) were determined as a function of the stress intensity amplitude ( $\Delta K$ ).  $\Delta K$ -control was employed during FCGR testing to achieve reasonably short test periods. Applied load was increased by a positive K-gradient of  $0.15 \text{ mm}^{-1}$ . Cyclic loading was sinusoidal, and the min/max load ratio R, was maintained at 0.1 throughout testing. Baseline FCGR tests were performed in laboratory air of low relative humidity (western U.S. environment) at 10 Hz loading frequency. Subsequent tests were performed in several testing solutions, including: simulated fuel grade ethanol (SFGE), and a different ethanol solution, prepared as a control (containing no microbes), and inoculated with active microbiological species. C(T) specimens were precracked in air until approximately 3 mm of crack length was achieved. Precracks were measured with an optical comparator and then submerged in test solutions under free-corrosion conditions. A reaction frame was constructed to perform the testing in the solutions contained in an inert polymer tank. The test chamber was approximately 6 L in volume and was sealed with gaskets to minimize evaporation of test solutions. After sample submersion, additional precracking cycles were performed in test solutions for a period of approximately 24 h prior to commencing FCGR tests. Precracking in solutions was performed at R=0.1, 0.1 Hz loading frequency, and with end  $\Delta K$  value less than initial  $\Delta K$  values for FCGR measurements. C(T) specimen dimensions, test parameters, and environmental conditions are shown in Table 2. FCGR testing was performed at 0.1 Hz in test solutions to allow for mass-transport corrosion processes at the crack tip. All mechanical testing was performed at room temperature (approximately 21 °C).

**Figure 1: Representative microstructures of as-received X52 (left) and X70 (right) pipeline steels.**

**Table 2: Fatigue Crack Growth Rate Test Parameters and Environmental Conditions**

Test Parameters		
Relevant C(T) Specimen Dimensions: W=50.8 mm, B=5.72 mm, H=30.48 mm		
Constant Load Ratio, R=0.1    Test Control, $\Delta K$ -increasing    Normalized K-Gradient, C=0.15 mm <sup>-1</sup>		
Test Solution Volume, 6 L		
Specimen	Test Environment	Frequency [Hz]
X52-2	Laboratory air – ambient conditions	10
X52-4	SFGE – 98.5 % ethanol, 1.0 % D.I. water, 0.5 % methanol, 56 mg/L acetic acid, 32 mg/L Cl <sup>-</sup>	0.1
X52-6	Ethanol solution (5 % ethanol, 1g/L NaCl, 0.5 g/L yeast extract, 0.3 g/L peptone, 1 g/L glutaraldehyde)	0.1
X52-5	Ethanol solution + <i>Acetobacter acetii</i>	0.1
X70-1	Laboratory air – ambient conditions	10
X70-3	SFGE – 98.5 % ethanol, 1.0 % D.I. water, 0.5 % methanol, 56 mg/L acetic acid, 32 mg/L Cl <sup>-</sup>	0.1
X70-4	SFGE – 98.5 % ethanol, 1.0 % D.I. water, 0.5 % methanol, 56 mg/L acetic acid, 32 mg/L Cl <sup>-</sup>	0.01, 0.1, 0.3, 0.6
X70-5	Ethanol solution (5 % ethanol, 1g/L NaCl, 0.5 g/L yeast extract, 0.3 g/L peptone)	0.1
X70-2	Ethanol solution + <i>Acetobacter acetii</i>	0.1
X70-6	Ethanol solution + <i>Acetobacter acetii</i>	0.1

Microbiological species including *Acetobacter acetii* and *Desulfosporosinus sp.*, were isolated from industrial ethanol storage tank samples. *Acetobacter acetii* oxidize ethanol into acetic acid during their life cycle. The *Desulfosporosinus sp.* is a sulfate reducing species (SRB). SRB are widely known to promote hydrogen damage in metals. Fatigue experiments with SRB are currently under investigation, and results will be reported in the future. *Acetobacter acetii* were inoculated into test solutions in a controlled laboratory environment. Cell counts were monitored until equilibrium cell concentrations were achieved, *i.e.*, the rate of bacterial growth was equal to the death rate. Microbe cell counts were performed with standard optical cell-counting methods during inoculation and growth of cultures in test solutions and throughout FCGR testing. Solution acidity was measured with a pH probe at both the start and the end of FCGR testing.

## RESULTS AND DISCUSSION

### Baseline Mechanical Properties

Mechanical properties including yield strength tensile strength, and elongation are shown in Table 3. Three tensile tests were performed for each alloy. Average values of strength and elongation were calculated from the three test runs and are reported along with the standard deviation ( $\delta$ ).

**Table 3: Mechanical Properties of Pipeline Steels**

Alloy	0.2 % Offset Yield Strength [MPa]		Ultimate Tensile Strength [MPa]		Total Elongation [%]	
	Average	$\delta$	Average	$\delta$	Average	$\delta$
X52	397	4.2	491	1.0	21.3	0.2
X70	561	14.5	655	9.1	17.2	0.8

Reference FCGRs determined in the laboratory air environment are plotted in Figure 2. The crack growth rate per loading cycle ( $da/dN$ ) is plotted as a function of stress intensity amplitude ( $\Delta K$ ) at the tip of the growing crack. Note that the X70 steel had lower crack growth rates at all levels of stress intensity. The finer-grained X70 steel would be expected to resist fatigue crack propagation more than X52, because it is widely accepted that increases in grain size generally result in reduction of fatigue performance. These data are useful to evaluate any changes in cracking behavior due to exposure to ethanol fuels and/or microbiological species. Note that crack growth rates were not determined near threshold (Stage I), because it is often assumed that structures contain some crack-like features (such as those produced during welding or surface flaws) when placed into service. The growth rates over the range of  $\Delta K$ -values evaluated were fitted with linear segments to determine Paris Law coefficients. The X52 data were fitted by a single segment, and the X70 data were fitted with two segments, with a transition at approximately  $30 \text{ MPa}\cdot\text{m}^{1/2}$ . A previous report on crack growth behavior of X70 also exhibited this transition in FCGR at a  $\Delta K$  value of approximately  $30 \text{ MPa}\cdot\text{m}^{1/2}$  [18]. Paris Law equations, determined by least-squares linear regression, are shown on Figure 2 for each region.

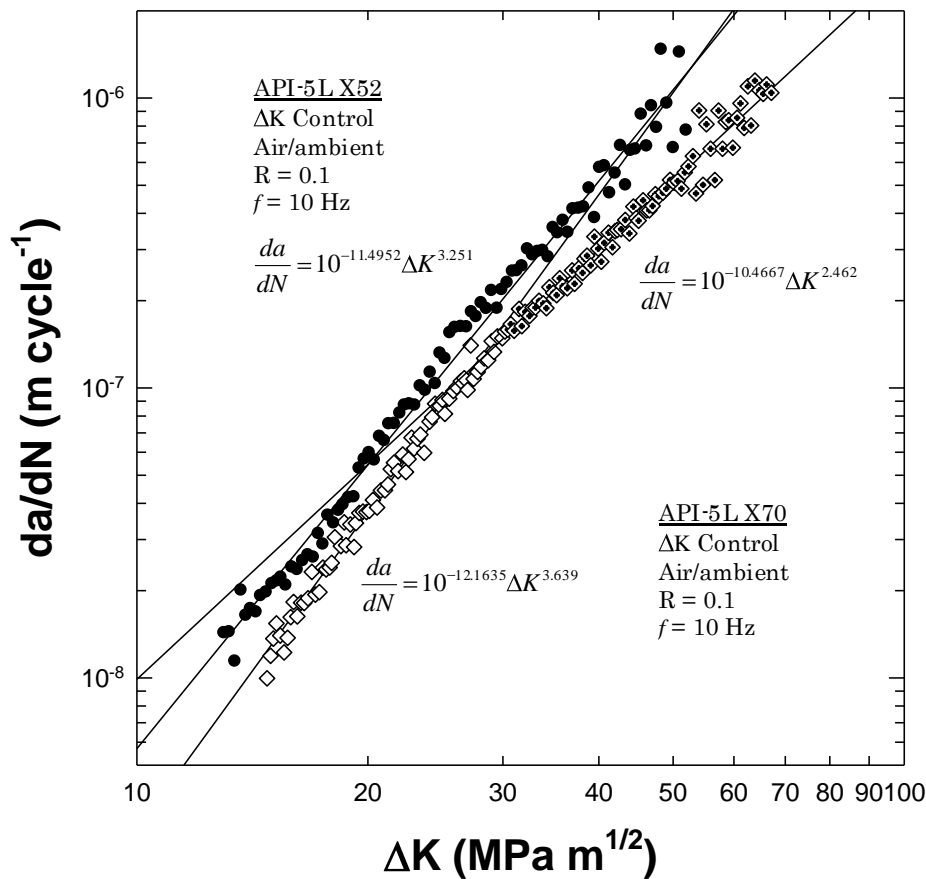


**Figure 2: Fatigue crack growth rates of X52 (●) and X70 (◇ <  $30 \text{ MPa}\cdot\text{m}^{1/2}$ , and ◇ >  $30 \text{ MPa}\cdot\text{m}^{1/2}$ ) in ambient conditions.**

### Simulated Fuel Grade Ethanol

As a precursor to evaluating the effects of microbiological life in ethanol fuels on corrosion-induced cracking, studies were performed to determine the effect of simulated fuel grade ethanol (SFGE) on FCGR. A solution of SFGE was mixed according to other stress corrosion cracking studies of pipeline steel in ethanol published in the literature (see Ref. [8], for example). The solution composition is given in Table 2.

FCGRs were determined in SFGE at similar stress intensity levels reported for the air data shown in Figure 2. However, tests were conducted at a lower cyclic loading frequency, to account for time-dependent corrosion processes occurring at the growing crack tip. Such low loading frequencies may be expected due to cyclic pressure fluctuations in a transport pipeline. Other test variables employed during the baseline testing protocol were maintained ( $R=0.1$ ,  $\Delta K$ -control, etc.). FCGRs of X52 and X70 measured in the various ethanol test solutions are presented in Figure 3. The presence of SFGE at the crack increased crack growth rates at stress intensity levels above approximately  $17 \text{ MPa}\cdot\text{m}^{1/2}$  and  $22 \text{ MPa}\cdot\text{m}^{1/2}$  in X52 and X70, respectively. These increases are due to corrosion fatigue, which is fatigue crack growth accelerated by a corrosion process. At the low stress-intensity levels, there appears to be no significant contribution of SFGE on crack growth behavior. True corrosion fatigue occurs below the critical stress intensity for stress corrosion cracking (SCC), *i.e.*, the  $K_{ISCC}$  value. A stress corrosion fatigue (SCF) mechanism would be expected at (and above) the  $K_{ISCC}$  value. Values of  $K_{ISCC}$  measured for pipeline steel tested in ethanol fuels have been reported elsewhere ( $33 \text{ MPa}\cdot\text{m}^{1/2}$  to  $35 \text{ MPa}\cdot\text{m}^{1/2}$  [5]). At a stress intensity ratio ( $R=K_{min}/K_{max}$ ) of 0.1, an SCF cracking mechanism would be expected at  $\Delta K$ -levels above approximately  $30 \text{ MPa}\cdot\text{m}^{1/2}$ , because  $\Delta K = (1-R)\cdot K_{max}$ . The most significant increase in crack growth of X70 in SFGE compared to values in air was observed at  $\Delta K \approx 30 \text{ MPa}\cdot\text{m}^{1/2}$ . The  $da/dN$  is over 90 % higher in SFGE than in air at this  $\Delta K$  value. FCGR increases were also observed during testing of X52 in SFGE, although they were not as significant as those observed in X70. Increases up to ~25 % greater were observed in the range of  $25 \text{ MPa}\cdot\text{m}^{1/2}$  to  $30 \text{ MPa}\cdot\text{m}^{1/2}$ , corresponding to  $K_{max}$  values of  $27.8 \text{ MPa}\cdot\text{m}^{1/2}$  to  $33.3 \text{ MPa}\cdot\text{m}^{1/2}$ , respectively.

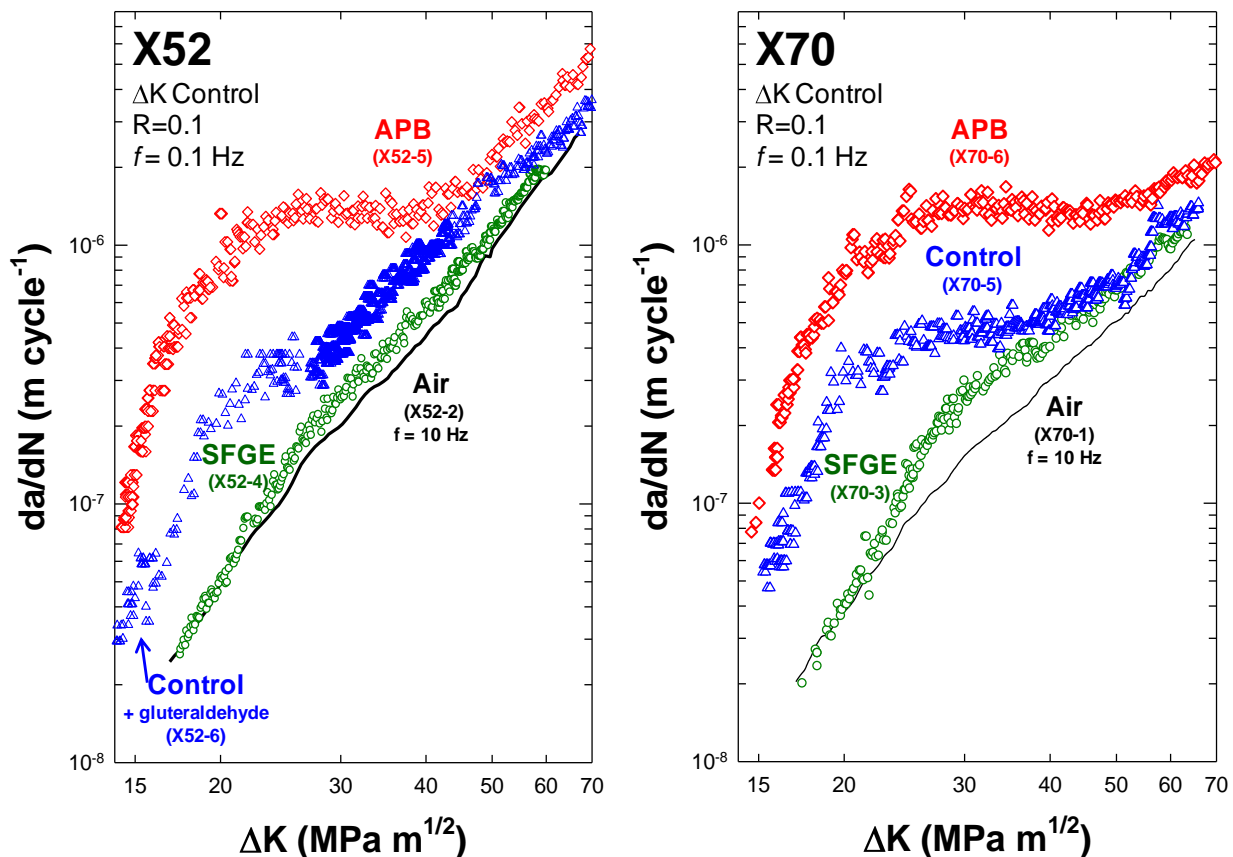


Figure 3: Fatigue crack growth rates of X52 (left) and X70 (right) in air (10 Hz) and other ethanol fuel test solutions (0.1 Hz).

Relative changes in the magnitude of crack growth increase are shown in Table 4 at increasing levels of  $\Delta K$  (and  $K_{max}$ ). The increase in  $da/dN$  caused by SFGE is greatest at (or near) the  $K_{ISCC}$  value ( $\sim 33$  MPa·m<sup>1/2</sup>). However, the increase in  $da/dN$  due to SFGE decreases above  $K_{ISCC}$ . SCC and SCF mechanisms require the presence of a stable passive surface film at the growing crack tip, in addition to tensile stress and a corrosive environment. SCF conditions are likely to be satisfied for values of  $K_{max}$  where  $da/dN$  increases were highest. As  $K_{max}$  increases above  $K_{ISCC}$ , stable surface films rupture to a greater extent, thus lessening the aggressiveness of a stress corrosion cracking mechanism, since the kinetics of passive film formation may not keep up with an advancing crack front. Decreasing surface coverage of passive film would prevent an aggressive localized attack and shift any observed increase of  $da/dN$  caused by SFGE towards more general mechanical and corrosion damage mechanisms. At the higher stress intensities evaluated, the crack growth rates in air and in SFGE converge. Mechanical damage at these stress intensity levels would dominate over corrosion damage, and crack growth rates in SFGE would be expected to converge with those found in air. Metallurgical evaluation of fracture surfaces will provide additional insight on the fracture behavior.

Cyclic loading frequency can have an effect on the crack growth rates measured during corrosion fatigue experiments<sup>[19]</sup>. The relationship between loading frequency and  $da/dN$  of X70 was determined in the SFGE solution at two constant levels of stress intensity amplitude. Results of these experiments are shown in Figure 4. Levels of maximum stress intensity were selected based on the clear effect of accelerated crack growth from corrosion processes relative to air (shown in Table 4). Maximum crack growth rates were found at 0.01 Hz, and those rates decreased slightly when increasing the test frequency to 0.1 Hz. A test frequency of 0.3 Hz still showed some influence of corrosion on crack growth rates, although significantly reduced from that at 0.1 Hz. At 0.6 Hz, the crack growth rate ( $K_{max} = 40$  MPa·m<sup>1/2</sup>) approached that of the test conducted in laboratory air. The dependency of  $da/dN$  with test frequency is a consequence of mass transport and reaction kinetics<sup>[19]</sup>. Fatigue testing period becomes prohibitively long at lower test frequencies. Therefore it was deemed that 0.1 Hz would be adequate to evaluate time-dependent corrosion phenomenon, while maintaining test periods to less than approximately 10 days.

**Table 4: Comparison of Crack Growth Rates in Air and SFGE**

$\Delta K$ [MPa·m <sup>1/2</sup> ]	$K_{max}$ [MPa·m <sup>1/2</sup> ]	da/dN in Air [m/cycle]		da/dN in SFGE [m/cycle]		FCGR Increase [%]	
		X52	X70	X52	X70	X52	X70
17	18.9	$2.53 \times 10^{-8}$	$2.03 \times 10^{-8}$	$2.60 \times 10^{-8}$	$2.00 \times 10^{-8}$	2.7	-
20	22.2	$4.94 \times 10^{-8}$	$3.82 \times 10^{-8}$	$5.05 \times 10^{-8}$	$3.86 \times 10^{-8}$	2.2	1.0
25	27.8	$1.10 \times 10^{-7}$	$8.64 \times 10^{-8}$	$1.49 \times 10^{-7}$	$1.14 \times 10^{-7}$	26.2	31.4
30	33.3	$2.01 \times 10^{-7}$	$1.53 \times 10^{-7}$	$2.65 \times 10^{-7}$	$2.97 \times 10^{-7}$	24.2	94.5
35	38.9	$3.04 \times 10^{-7}$	$2.17 \times 10^{-7}$	$3.95 \times 10^{-7}$	$3.65 \times 10^{-7}$	23.0	68.3
40	44.4	$4.46 \times 10^{-7}$	$3.02 \times 10^{-7}$	$5.96 \times 10^{-7}$	$4.01 \times 10^{-7}$	25.2	45.0
45	50.0	$6.26 \times 10^{-7}$	$3.98 \times 10^{-7}$	$7.84 \times 10^{-7}$	$5.51 \times 10^{-7}$	20.2	38.5
50	55.6	$9.70 \times 10^{-7}$	$5.06 \times 10^{-7}$	$1.17 \times 10^{-6}$	$6.64 \times 10^{-7}$	17.1	31.3
55	61.1	-	$6.36 \times 10^{-7}$	$1.55 \times 10^{-6}$	$8.35 \times 10^{-7}$	-	31.3
60	66.7	-	$8.07 \times 10^{-7}$	$1.94 \times 10^{-6}$	$9.63 \times 10^{-7}$	-	19.3
65	72.2	-	$1.05 \times 10^{-6}$	-	$1.09 \times 10^{-6}$	-	4.2

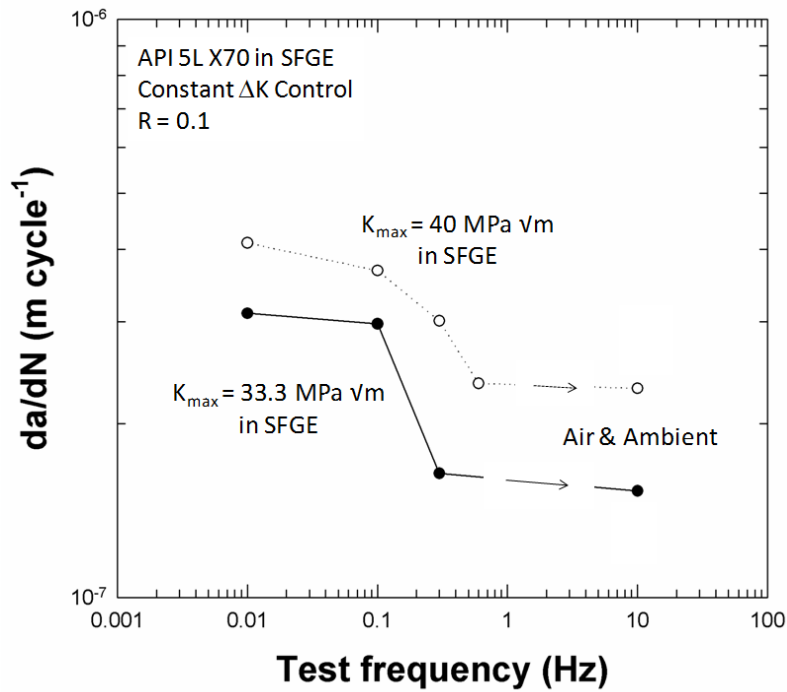


**Figure 4: Effect of loading frequency on crack growth rates for two constant stress intensity amplitudes. Crack growth rates obtained at 10 Hz were determined in air.**

Figure 5 shows opposing fracture surfaces of the X52 FCGR test specimen performed in SFGE. After  $da/dN$  testing was completed, the C(T) specimens were overloaded to  $K_{IC}$  levels so that fracture surfaces could be examined. Values of  $\Delta K$  are shown along the length of the crack in approximate locations. Crack advance was from the right side to the left in the image. Note that corrosion product is present along much of the fracture surface. It is most pronounced after the precrack, i.e., during the  $da/dN$  portion of the test. No observable corrosion product was apparent in macroscopic views at crack lengths coinciding with  $\Delta K$  levels of  $\sim 60 \text{ MPa}\cdot\text{m}^{1/2}$  or greater. Mechanical damage tends to dominate the crack growth in this stress-intensity regime, as discussed previously. Fracture examination of the X70 FCGR test specimen revealed a similar appearance. However, the X70 crack front was significantly curved. This was a common observation among all X70 tests specimens. Uneven crack advance was likely a consequence of nonuniform residual stresses induced during pipe forming. Cracks advanced faster on the side of the C(T) specimen coinciding with the outer diameter of the pipe from which it was sectioned. Crack fronts apparently reached a condition of relatively uniform advance, although they maintained their curvature. Curvature likely induces error in the measurement of crack length with the compliance method, although probably not to a great extent, as discussed below.

Surfaces of test specimens were evaluated for corrosion damage induced by the SFGE environment. Micrographs of as-tested C(T) specimen surfaces in the region containing the crack are shown in Figure 6. Surface pitting was observed on X52 and X70 specimens after testing. Pit diameters ranged from a few micrometers up to approximately  $25 \mu\text{m}$ . Pits were slightly larger on X52 specimens, and appeared to be associated with selective attack of pearlite colonies. Pits also tended to be wider and shallower in X52 than X70. Initiation of pits on X70 may have taken place at inclusion sites or at fine-scale carbides, hence their smaller size. Chloride and dissolved oxygen have been shown to increase pitting susceptibility of steel in SFGE [7]. Chloride was present as an additive in the SFGE, and dissolved oxygen was available since the bulk solution was exposed to air. Additional aeration may have occurred due to mechanical agitation of the solution throughout testing. It is noteworthy that the X52 appears to be more susceptible to pitting in SFGE based on pit size alone.

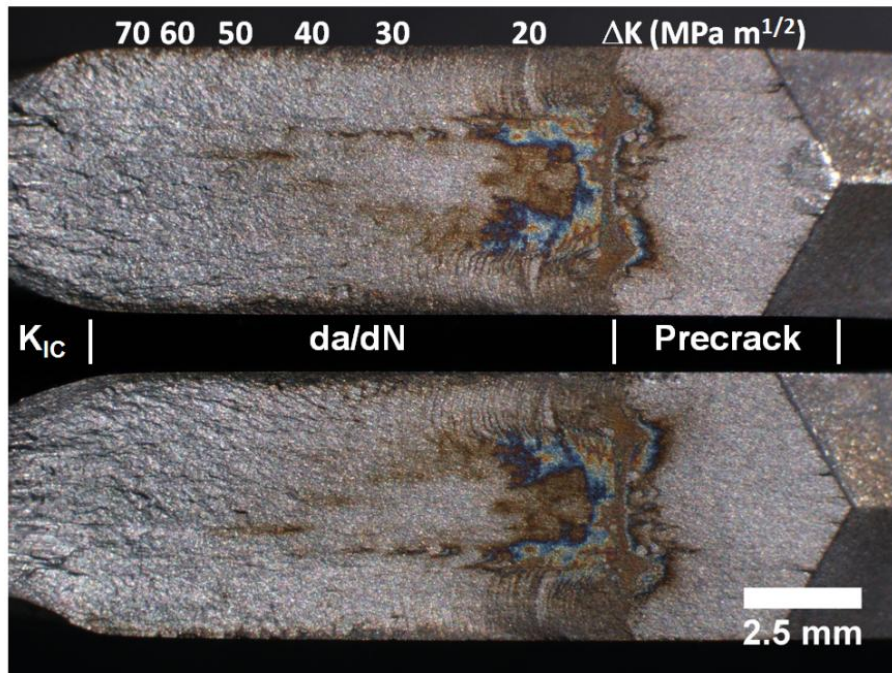


**Figure 5: Opposing fracture faces of an X52 specimen after FCGR testing in SFGE.**

Regions adjacent to the cracks were polished to evaluate fracture morphology. Fractures appeared to be exclusively transgranular at all levels of  $\Delta K$  in both materials. Microstructural regions adjacent to the crack at intermediate levels of  $\Delta K$  are shown Figure 6. Note that some corrosion product is evident along the secondary fracture in X70. These products, observed along fracture surfaces of both steels, were typically reddish-brown or black, corresponding to  $\text{Fe}(\text{OH})_3$  and  $\text{Fe}_3\text{O}_4$ , respectively. Crystallographic analysis would be necessary to substantiate the presence of these corrosion products. SCC fractures of pipeline steel in SFGE have been reportedly transgranular in morphology<sup>[3,8]</sup>. SCC in SFGE initiates due to localized film breakdown, and then propagation commences from the competition between anodic dissolution and repassivation ahead of the growing crack<sup>[5,8]</sup>. SCC and corrosion fatigue share some of the common damage mechanisms including *hydrogen embrittlement* and *film rupture, dissolution and repassivation*<sup>[19]</sup>. It is likely that corrosion fatigue damage of X52 and X70 in SFGE is a *film rupture, dissolution and repassivation* mechanism, based on previous explanations of ethanol SCC.

A comparison of X52 and X70  $da/dN$  data suggests that there may be a strength dependency of FCGRs in SFGE; that is, materials with higher yield strength may be more susceptible to corrosion fatigue. A strength dependency suggests that a hydrogen embrittlement mechanism induces corrosion fatigue damage. Such a mechanism has been proposed for high-strength steel in ethanol-water mixtures<sup>[15]</sup>. However, ethanol is a very weak acid and does not dissociate to an appreciable level. It is perhaps more likely that there is a microstructural influence on the corrosion damage mechanism. Newman discussed that carbides act as electrocatalyst sites for oxidation of alcohols<sup>[6]</sup>. Note that the X70 composition (Table 1) has a significantly higher concentration of carbide-forming elements (Cr, Mo, Nb, Ti, and V) than X52. A finer and denser dispersion of carbides would be expected in X70, and would lead to a higher carbide surface coverage at freshly exposed metal near the crack tip. According to Newman's proposed mechanism<sup>[6]</sup>, this could promote oxidation of alcohol into [acetic] acid at the freshly exposed metal of an incrementally-growing crack tip. This observation warrants additional investigation, since little is known about carbide catalysts for ethanol oxidation<sup>[6]</sup>. Acetic acid plays an important role in APB corrosion as discussed in the next section.

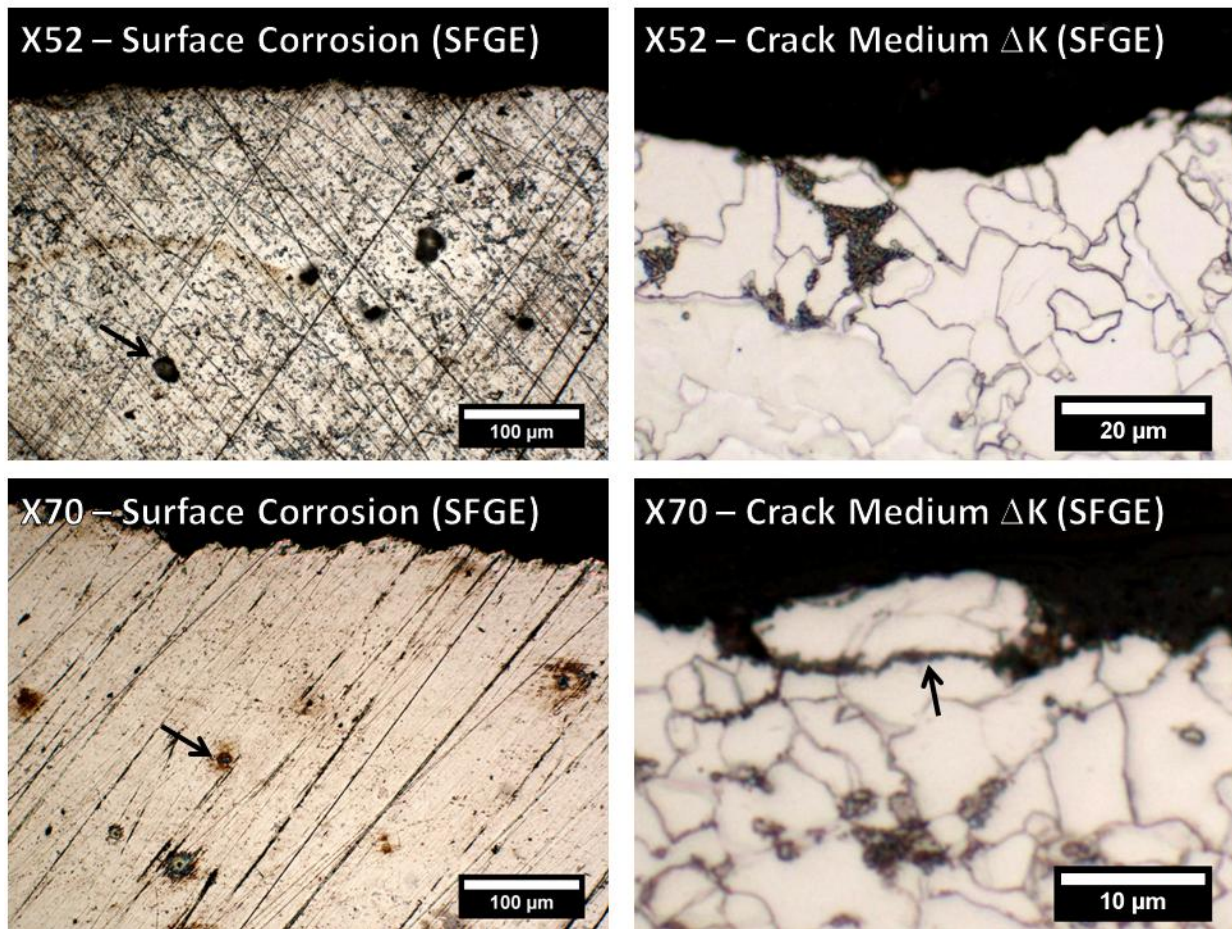


**Figure 6: Surface corrosion (left) and crack morphology (right) of X52 (top) and X70 (bottom) C(T) specimens after FCGR testing in SFGE. Pitting and intragranular fractures are indicated with arrows.**

### Acid Producing Bacteria

FCGRs of X52 and X70 in the various ethanol test solutions were presented in Figure 3 and a discussion of the SFGE has been provided. FCGRs were significantly higher in SFGE (relative to air) but are drastically higher in the ethanol test solution inoculated with APB. A significant slope transition occurs in the FCGR data of the inoculated solution at approximately  $20 \text{ MPa}\cdot\text{m}^{1/2}$ . It is noteworthy that the general shape and scale of the  $da/dN$  curves is the same in X52 and X70 up to a  $\Delta K \approx 50 \text{ MPa}\cdot\text{m}^{1/2}$ . Slopes of both APB  $da/dN$  data sets vary significantly through the stress intensity range of  $20 \text{ MPa}\cdot\text{m}^{1/2}$  to  $50 \text{ MPa}\cdot\text{m}^{1/2}$ , indicating a wide variation in Paris Law exponents. Crack growth rates in APB solution were almost two orders of magnitude higher than in air, as shown in a summary of FCGR numerical values in Table 5. Water concentration was higher in the ethanol test solutions than would be permitted in a fuel blend in order to promote microbial growth. However, ethanol is hygroscopic and upset conditions of high water content may be expected near the bottom of an ethanol pipeline, due to its higher density. Such conditions may be favorable for APB to thrive.

**Table 5: Comparison of Crack Growth Rates in Air and APB Solution**

$\Delta K$ [MPa·m <sup>1/2</sup> ]	$K_{max}$ [MPa·m <sup>1/2</sup> ]	da/dN in Air [m/cycle]		da/dN in APB [m/cycle]		FCGR Increase [%]	
		X52	X70	X52	X70	X52	X70
17	18.9	2.53 x 10 <sup>-8</sup>	2.03 x 10 <sup>-8</sup>	4.91 x 10 <sup>-7</sup>	3.28 x 10 <sup>-7</sup>	1,841	1,516
20	22.2	4.94 x 10 <sup>-8</sup>	3.82 x 10 <sup>-8</sup>	1.32 x 10 <sup>-6</sup>	7.80 x 10 <sup>-7</sup>	2,572	1,942
25	27.8	1.10 x 10 <sup>-7</sup>	8.64 x 10 <sup>-8</sup>	1.22 x 10 <sup>-6</sup>	1.62 x 10 <sup>-6</sup>	1,009	1,775
30	33.3	2.01 x 10 <sup>-7</sup>	1.53 x 10 <sup>-7</sup>	1.37 x 10 <sup>-6</sup>	1.39 x 10 <sup>-6</sup>	582	808
35	38.9	3.04 x 10 <sup>-7</sup>	2.17 x 10 <sup>-7</sup>	1.12 x 10 <sup>-6</sup>	1.36 x 10 <sup>-6</sup>	268	527
40	44.4	4.46 x 10 <sup>-7</sup>	3.02 x 10 <sup>-7</sup>	1.27 x 10 <sup>-6</sup>	1.24 x 10 <sup>-6</sup>	185	311
45	50	6.26 x 10 <sup>-7</sup>	3.98 x 10 <sup>-7</sup>	1.62 x 10 <sup>-6</sup>	1.45 x 10 <sup>-6</sup>	159	264
50	55.6	9.70 x 10 <sup>-7</sup>	5.06 x 10 <sup>-7</sup>	2.24 x 10 <sup>-6</sup>	1.48 x 10 <sup>-6</sup>	131	192
55	61.1	-	6.36 x 10 <sup>-7</sup>	3.10 x 10 <sup>-6</sup>	1.55 x 10 <sup>-6</sup>		144
60	66.7	-	8.07 x 10 <sup>-7</sup>	3.38 x 10 <sup>-6</sup>	1.78 x 10 <sup>-6</sup>		121
65	72.2	-	1.05 x 10 <sup>-6</sup>	4.08 x 10 <sup>-6</sup>	2.04 x 10 <sup>-6</sup>		94

Acidity values and results of bacteria cell counts of the APB test solutions are included in Table 6. The values represent test solution conditions at the start and end of the FCGR test. *Acetobacter aceti* oxidized ethanol into acetic acid and lowered the pH of the test solutions from a “control” solution pH of approximately 6.6. Note that pH changed very little during the course of both tests in APB solutions, even though bacterial counts increased somewhat. Some fluctuation in bacterial counts was expected in the steady-state bacterial-growth region. Pitting susceptibility of steel in SFGE is known to decrease with increasing H<sub>2</sub>O content [7]. Based on that finding, and the fact that APB solutions in this study had high water and low ethanol concentrations, the pitting behavior observed on C(T) specimens (shown in Figure 8) can likely be attributed to the presence of acetic acid. Acetic acid produced by bacteria was shown to attack the matrix of pipeline steel at inclusion sites, resulting in a deep pitting corrosion [12]. A similar deep pitting behavior was observed on C(T) specimens, as shown in Figure 7.

**Table 6: Cell Count and pH Values Measured during APB and Control Tests**

Test	Initial Cell Count [#/mL]	Final Cell Count [#/mL]	Initial Solution Acidity [pH]	Final Solution Acidity [pH]
X70-6 (APB)	2.10 x 10 <sup>7</sup>	2.80 x 10 <sup>7</sup>	3.60	3.58
X70-5 (Control – no inoculation)	0	9.10 x 10 <sup>6</sup>	6.60	4.82
X52-5 (APB)	2.28 x 10 <sup>7</sup>	2.90 x 10 <sup>7</sup>	3.35	3.36
X52-6 (Control + glutaraldehyde)	0	-	6.5*	6.5*

\*Values are approximate and were measured with pH paper

As in the case of SFGE, crack morphology was found to be transgranular in nature. Representative crack edges are shown in Figure 7. Significant amounts of corrosion products were present along the fractures of the APB tests. This observation is also consistent with the surface appearance of test specimens, which contained copious amounts of corrosion product. Figure 8 shows an SEM image of a biofilm that grew on a laboratory immersion test sample in APB solution. The biofilm was later removed to reveal the corrosion damage on the sample surface, which is also shown in Figure 8. Biofilms are expected to modify electrochemical processes and promote formation of differential aeration cells that promote pitting [11]. Morphology of the biofilm and corrosion damage on the C(T) specimen surfaces are expected to be similar in nature to the laboratory immersion test.

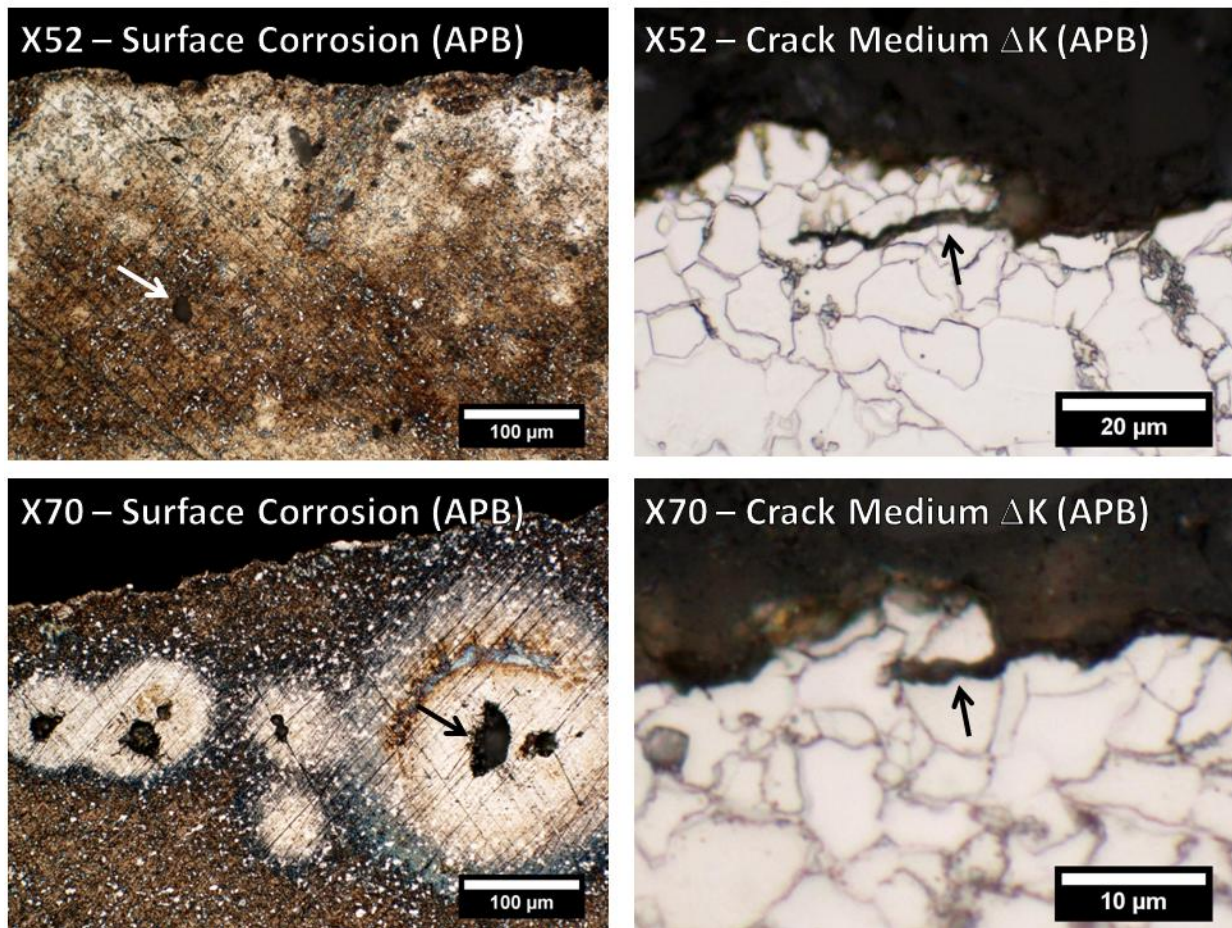


**Figure 7: Surface corrosion (left) and crack morphology (right) of X52 (top) and X70 (bottom) C(T) specimens after FCGR testing in APB. Pitting and intragranular fractures are indicated with arrows.**

X70 FCGRs were measured in an ethanol test solution “control” that was not inoculated with microbiological species. The control solution contained ethanol, water, chloride, yeast extract, and peptone. A previous report indicated that increases in the water content of ethanol increased FCGR<sup>[15]</sup>. While it is known that chloride can influence the crack growth rates, an effect of yeast extract and peptone on FCGRs is not expected. Differentiation between the effect of the high water content in the ethanol solutions, which promotes fervent microbiological growth, and the effect of the microbes themselves was the basis for a control test. However, the species *Acetobacter aceti* is abundant throughout nature. This natural abundance made it difficult to run a true control solution, as evident from the initial attempt to evaluate X70 (test X70-5 in Figure 3). Cell counting after the X70-5 test showed a significant concentration of APB cells, albeit at a concentration an order of magnitude lower than that of the inoculated solutions. This concentration was enough to lower pH from approximately 6.60 (control condition) to 4.82 after contamination. Still, the FCGRs in this solution were much lower than in the inoculated APB solution. Glutaraldehyde has seen use as an effective biocide in oil and gas operations. It was included in a test of X52 in another control to determine its effectiveness on preventing growth of the APB. Results from the experiment containing glutaraldehyde additions (X52-6) were promising in that FCGRs were lower than in the APB solution (X52-5) and the X70 control test (X70-5) as shown in Figure 3. Acidity level did not change significantly during the control test containing the biocide glutaraldehyde (X52-6) even though *Acetobacter aceti* are ubiquitous, and readily contaminated the X70-5 control test.

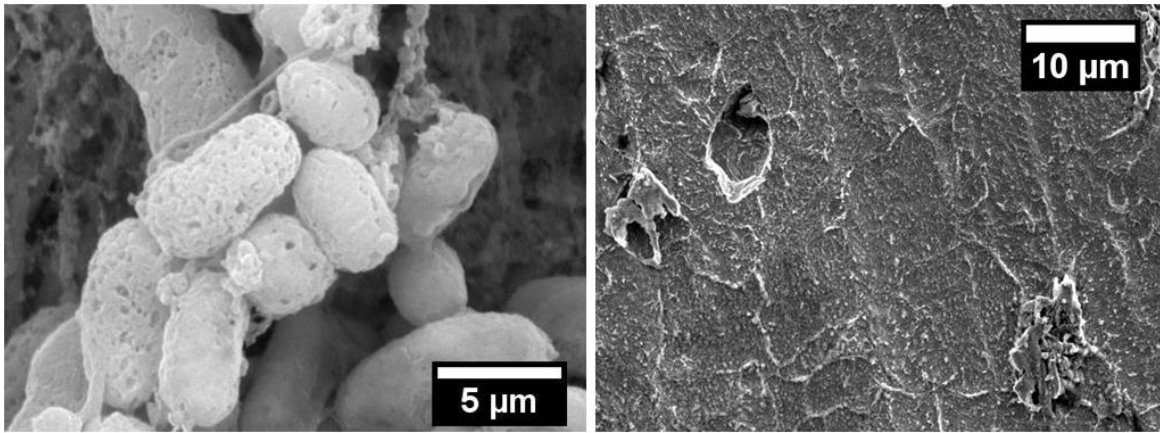


**Figure 8: Scanning electron micrographs of APB biofilm on X52 laboratory immersion specimen (left), and pitting induced by APB on X52 (right).**

Figure 9 shows opposing fracture surfaces of the X70 FCGR test performed in APB solution. Note the curvature of the crack front after precracking and throughout the  $da/dN$  portion of testing. A discussion above indicated uneven growth of the crack front was probably induced by nonuniform residual stresses across the pipe wall thickness. These nonuniform stresses could introduce error into measurement of crack length with the compliance technique. A comparison of FCGR data from the current study with earlier experiments<sup>[18]</sup> was performed to see whether significant differences in FCGR were apparent. Figure 10 shows that FCGRs in air were similar to those measured in earlier experiments, and probably within typical measurement uncertainty of  $da/dN$  data. Fatigue-crack growth rates were also determined in air and 3.5 % NaCl solution at two corrosion potentials in the earlier experiments, with a constant load ratio of 0.05 and triangular waveform loading<sup>[18]</sup>. Note the similarity in FCGRs of X70 in APB solution from the current work and 3.5 % NaCl solution from the earlier experiments.

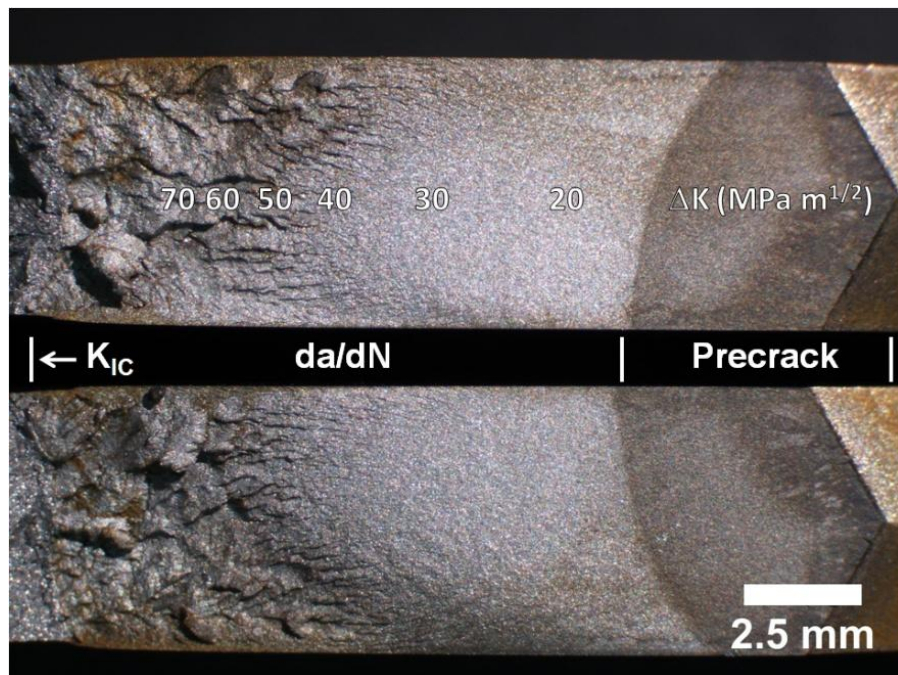


**Figure 9: Opposing fracture faces of an X70 specimen after FCGR testing in APB solution.**

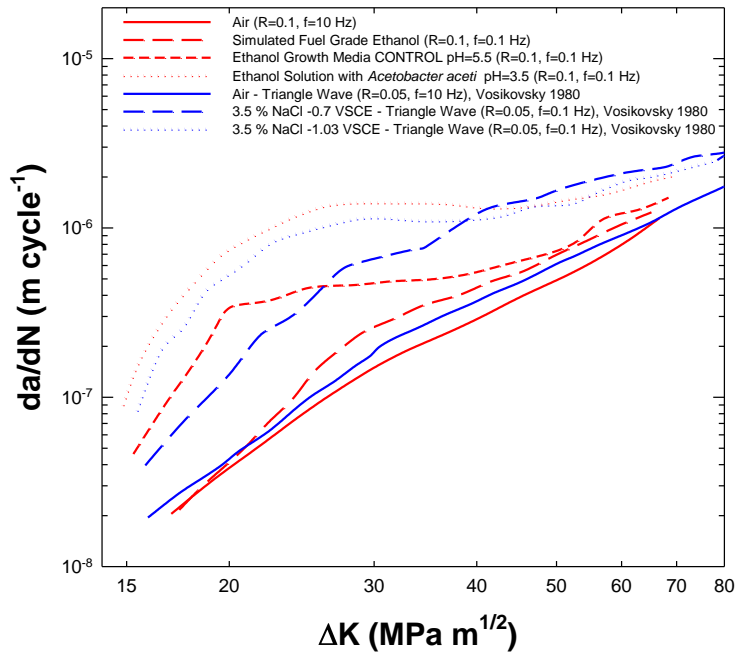


Figure 10: Comparison of X70 FCGR in ethanol solutions with data from previous fatigue experiments<sup>[18]</sup> of X70 in 3.5 % NaCl aqueous solutions.

## CONCLUSIONS

Fatigue crack growth rates were determined for two pipeline steel alloys as a function of  $\Delta K$  in the following environments, which are ranked in ascending order of potential to aggravate crack growth rates: laboratory air, simulated fuel grade ethanol, ethanol solution for bacterial growth, and ethanol solution inoculated with the acid producing bacteria *Acetobacter acetii*. The following conclusions can be made based on this work:

- Crack growth rates of X70 were generally lower than those of X52 in all environments. An exception to this was observed during testing of X70 in SFGE near  $K_{ISCC}$  ( $\sim 33 \text{ MPa}\cdot\text{m}^{1/2}$ ).
- Crack growth rates were found to be significantly higher in simulated fuel grade ethanol, relative to air, in the  $\Delta K$  range of  $25 \text{ MPa}\cdot\text{m}^{1/2}$  to  $65 \text{ MPa}\cdot\text{m}^{1/2}$ . Accelerated crack growth rates may be attributed to corrosion fatigue and/or stress corrosion fatigue mechanisms, although characterization work is required on fractured specimens to better explain the accelerated behavior.
- Although stress corrosion fatigue processes are time-dependent, a frequency of 0.1 Hz provides a compromise between maintaining acceptably short test times, and adequately characterizing corrosion-enhanced crack growth behavior in the presence of SFGE.
- APB produced acetic acid by oxidizing ethanol. Production of acetic acid lowered test solution pH and increased the FCGRs by over an order of magnitude at intermediate levels of  $\Delta K$ .
- Surface pitting occurred on C(T) specimens during FCGR testing in SFGE and APB solutions, although APB solutions promoted the most aggressive pitting, which may have been associated with the presence of a biofilm.
- Transgranular fatigue crack growth was the prevalent fracture morphology in SFGE and APB test environments.
- Preliminary testing in a control solution containing glutaraldehyde indicated that this compound may be an effective biocide for controlling APB growth in ethanol fuel environments since no drop in acidity was observed, *i.e.*, significant growth of APB cultures did not occur.

## ACKNOWLEDGEMENTS

We acknowledge technical assistance from others at NIST (Marc Dvorak, Elisabeth Mansfield, Ross Rentz, Mark Richards, and Ken Talley) and the Colorado School of Mines (Dave Olson, John Spear, and Brajendra Mishra). Financial support was provided by the U.S. Department of Transportation through the Pipeline and Hazardous Materials Safety Administration (Jim Merritt and Robert Smith). Work performed by J.W. Sowards was supported by an NRC Postdoctoral Fellowship at NIST-Boulder.

## REFERENCES

1. U.S. Energy Information Administration DOE/EIA-0484. "International Energy Outlook 2010" (Washington, DC: U.S. Department of Energy).
2. R. Kane, N. Sridhar, M. Brongers, J. Beavers, A. Agrawal, L. Klein, "Stress Corrosion Cracking in Fuel Ethanol: A Recently Recognized Phenomenon," *Materials Performance* 44, 12 (2005): pp. 50-55.
3. N. Sridhar, K. Price, J. Buckingham, J. Dante, "Stress Corrosion Cracking of Carbon Steel in Ethanol," *Corrosion* 62, 8 (2006): pp. 687-702.
4. X. Lou, D. Yang, P.M. Singh, "Effect of Ethanol Chemistry on Stress Corrosion Cracking of Carbon Steel in Fuel-Grade Ethanol," *Corrosion* 65, 12 (2009): pp. 785-797.
5. J.A. Beavers, F. Gui, N. Sridhar, "Effects of Environmental and Metallurgical Factors on the Stress Corrosion Cracking of Carbon Steel in Fuel-Grade Ethanol," *Corrosion* 67, (2011): doi:10.5006/1.3553341.
6. R.C. Newman, "Review and Hypothesis for the Stress Corrosion Mechanism of Carbon Steel in Alcohols," *Corrosion* 64, 11 (2008): pp. 819-823.
7. X. Lou, P.M. Singh, Role of Water, "Acetic Acid and Chloride on Corrosion and Pitting Behaviour of Carbon Steel in Fuel-Grade Ethanol," *Corrosion Science* 52, 7 (2010): pp. 2303-2315.
8. X. Lou, D. Yang, P.M. Singh, "Film Breakdown and Anodic Dissolution during Stress Corrosion Cracking of Carbon Steel in Bioethanol," *Journal of The Electrochemical Society* 157, 2 (2010): pp. C86-C94.
9. E.C. Hill, G.C. Hill, "Microbial Contamination and Associated Corrosion in Fuels, during Storage, Distribution and Use," *Advanced Materials Research* 38 (2008): pp. 257-268.
10. L. Jain, C. Williamson, S.M. Bola, R. Bola, J.R. Spear, B. Mishra, D.L. Olson, R. Kane, "Microbiological and Electrochemical Evaluation of Corrosion and Microbiologically Influenced Corrosion of Steel in Ethanol Fuel Environments," CORROSION/10, paper no. 10070 (Houston, TX: NACE, 2010).
11. B. Little, P. Wagner, F. Mansfield, "Microbiologically Influenced Corrosion of Metals and Alloys," *International Materials Review* 36, 6 (1991): pp. 253-272.
12. D.H. Pope, T.P. Zintel, A.K. Kuruvilla, O.W. Siebert, "Organic Acid Corrosion of Carbon Steel: A Mechanism of Microbiologically Influenced Corrosion," CORROSION/88, paper no. 79 (Houston, TX: NACE, 1988).
13. C.J. Thomas, R.G.J Edyvean, R. Brook, "Biologically Enhanced Corrosion Fatigue," *Biofouling* 1 (1988): pp. 65-77.

14. R.P. Gangloff, R.G. Kelly, "Microbe-enhanced Environmental Fatigue-Crack Propagation in HY-130 Steel," *Corrosion* 50, 5 (1994): pp. 345-354.
15. H. Ouchi, J. Kobayashi, I. Soya, K. Okamoto, "Fatigue Crack Growth in a High Tensile Strength Steel in Seawater and Several Other Environments," *ISIJ International* 34, 5 (1994): pp. 451-459.
16. ASTM E8 (09), "Standard Test Methods for Tension Testing of Metallic Materials" (West Conshohocken, PA: ASTM).
17. ASTM E647 (08), "Standard Test Method for Measurement of Fatigue Crack Growth Rates" (West Conshohocken, PA: ASTM).
18. O. Vosikovsky, "Effects of Stress Ratio on Fatigue Crack Growth Rates in X70 Pipeline Steel in Air and Saltwater," *Journal of Testing and Evaluation* 8, 2 (1980): pp. 68-73.
19. R.P. Gangloff, "Environmental Cracking – Corrosion Fatigue," MNL20-2ND, *Corrosion Tests and Standards: Application and Interpretation*, 2<sup>nd</sup> ed. (West Conshohocken, PA: ASTM, 2005)